Binding energies and structures of two-dimensional excitonic complexes in transition metal dichalcogenides

Daniel W. Kidd, David K. Zhang, and Kálmán Varga

Phys. Rev. B **93**, 125423 — Published 18 March 2016

DOI: 10.1103/PhysRevB.93.125423

Binding Energies and Structures of 2D Excitonic Complexes in Transition Metal Dichalcogenides

Daniel W. Kidd, David K. Zhang and Kálmán Varga

Department of Physics and Astronomy, Vanderbilt University, Nashville, Tennessee 37235, USA

The stochastic variational method is applied to excitonic formations within semiconducting transition metal dichalcogenides using a correlated Gaussian basis. The energy and structure of two- to six-particle systems are investigated along with their dependence on the effective screening length of the two-dimensional Keldysh potential and the electron-hole effective mass ratio. Excited state biexcitons are shown to be bound, with binding energies of the $L = 0$ state showing good agreement with experimental measurements of biexciton binding energies. Ground and newly discussed excited state exciton-trions are predicted to be bound and their structures are investigated.

I. INTRODUCTION

Much interest has been paid towards the research of two-dimensional (2D) materials ever since the isolation of graphene[1]. Such materials have exhibited behavior indicative of extraordinary potential functionality within nanoelectronics and photoelectronics[2–8]. While graphene spearheads this movement with its ideal electronic properties, its lack of a band gap limits its capabilities and motivates the search for an alternate semiconducting 2D material, i.e., a "graphene with a band gap"[9,10]. One popular family of candidate materials is that of the transition metal dichalcogenides (TMDs) which have been heavily investigated[11–14].

Such semiconducting materials occurring in 2D monolayers display a notably strong Coulomb interaction between charge carriers as a result of the reduced dimensionality[15]. This enhanced interaction, in turn, leads to the formation of tightly bound electron-hole pairs (excitons) with binding energies on the scale of several hundred milliectronvolts[16–19] — much greater than those in counterpart 3D materials. Futhermore, charged excitons (trions) have similarly been shown to form with significant binding energies in TMDs, including MoS_2 (20 meV)[20], WS_2 (45 meV)[21], and WSe_2 (30 meV)[22]. These surprisingly large binding energies imply that the formation of bound exciton pairs (biexcitons) may be possible, and so far these states have indeed been observed in WSe_2 (52 meV)[23] and WS_2 (65 meV)[24].

In order to characterize the optical and electrical responses of these materials and assess their potential functionality, one must thoroughly understand these excitonic formations. Effective mass models are commonly chosen to describe electron-hole systems[25–27] and have been widely employed towards such excitonic formations in 2D materials[28–31]. Most effective mass approaches use variational methods to calculate binding energies and wave functions, but the Path Integral Monte Carlo (PIMC) approach has also been recently applied to the geometry and energies of excitons, trions, and biexcitons within TMDs[32].

In a previous publication, we have shown that while the effective mass model correctly predicts the binding energies of excitons and trions within 2D materials, it fails to do so for biexcitons[33]. The model predicts that the biexciton is less strongly bound than the trion, in contradiction to experimental findings. This discrepancy has also been noted in other effective mass model calculations[34,35]. However, this is reconciled by the suggestion that the experimentally observed states are actually those of excited biexcitons, as opposed to ground state biexcitons.

In this paper, we study the effect that electron-hole effective mass ratio σ and the material indicative effective screening length r_0 have on the binding energies of these excitonic formations. We do so by means of fully analytical calculations without numerical approximation of the potential. High accuracy is necessary due to the particular nature of this potential and the extended geometry of the allowed bound states. We compare our results to other effective mass model studies[29,32,34,35], finding good agreement. Furthermore, we include the theoretical ground state energies of five- and six-body excitonic formations and show that while the five-body system remains bound (this is also concluded in Ref. 35), the six-body system is unbound. To the best of our knowledge, we are first in describing excited biexciton and exciton-trion states in 2D materials.

Our computations employ the stochastic variational method[36] applied to exciton ($X = eh$), trion ($X^- = eeh$), biexciton ($X_2 = eehh$), as well as five- and six-particle systems using an explicitly correlated Gaussian (ECG) basis. This basis has been previously shown to achieve accuracy of up to 8-10 digits when describing the binding energies of similar systems such as H_2[37], H_2^+, and the positronium molecule (Ps_2)[38,39]. This method has been shown to be well-suited for describing the binding energies of excitonic structures ranging from the two-body exciton to five-body exciton-trion systems[26,27,33]. Previously, we have shown that this method yields values that agree with experimental findings for the binding energies of excitons and trions within TMDs[33].

The paper is organized as follows. In section II we present the formalism describing our Hamiltonian and variational trial functions as well as the physical quantities to be extracted. Section III entails a comparison of

our results with those of other studies along with an extended listing of our results for varying r_0 and σ. Finally, in section IV, we provide concluding remarks.

II. FORMALISM

A. Hamiltonian and basis functions

The nonrelativistic Hamiltonian of an excitonic few-particle system is given by

$$H = \sum_{i=1}^{N} -\frac{1}{2m_i}\nabla_i^2 + \sum_{i<j}^{N} V(r_{ij}). \tag{1}$$

Note that the e-h exchange interaction[40] has been disregarded throughout the presented calculations. In the case of an excitonic system lying in a 2D plane, the interaction potential $V(r_{ij})$ is given by the 2D screened electrostatic interaction potential derived by Keldysh[28]

$$V(r_{ij}) = \frac{q_i q_j}{\kappa r_0} V_{2D}\left(\frac{r_{ij}}{r_0}\right), \tag{2}$$

where

$$V_{2D}(r) = \frac{\pi}{2}\left[H_0(r) - Y_0(r)\right]. \tag{3}$$

Here $\mathbf{r}_i$, m_i, and q_i are respectively the 2D position vector, effective mass, and charge of the ith particle, while $r_{ij} = |\mathbf{r}_i - \mathbf{r}_j|$ and r_0 is the screening length indicative of the medium. κ is the average environmental dielectric constant typically described as $\kappa = (1+\epsilon_{\text{env}})/2$, representing an environment of vacuum on one side and a substrate of dielectric constant ϵ_{env} on the other. Unless otherwise specified, throughout this paper the system is assumed to be suspended in vacuum with ϵ_{env} set to unity. H_0 and Y_0 are the Struve function and Bessel function of the second kind, respectively. In this form, the resulting energy of excitonic systems is a function of only r_0 and the electron-hole mass ratio $\sigma = m_e/m_h$.

The nonlocal macroscopic screening, inherent to 2D systems, distinguishes this potential from its 3D Coulombic counterpart[41]. The length scale of this screening is determined by the 2D layer polarizability χ_{2D} as $r_0 = 2\pi\chi_{2D}/\kappa$. In the limit of very strong screening ($r_0 \to \infty$), the potential exhibits a logarithmic divergence, while in the limit of small screening length ($r_0 \to 0$), $V(r_{ij})$ approaches the usual $1/r$ behavior of the Coulomb potential. In the latter case, the exact analytic solution for the single exciton energy is $E_X(r_0,\sigma)|_{r_0\to 0} = 2$ a.u. for a reduced mass of $\mu = 1$[30,32]. However, the corresponding energies for excitonic systems with more than two particles are not analytically available.

The variational method is used to calculate the energy of the system. As a trial function we choose a two dimensional (2D) form of the correlated Gaussians[42,43]:

$$\exp\left\{-\frac{1}{2}\sum_{i,j=1}^{N} A_{ij}\boldsymbol{\rho}_i\cdot\boldsymbol{\rho}_j\right\}, \tag{4}$$

where the nonlinear parameters are different and independent in both the radial and vertical direction. The above form of the CG belongs to $M = 0$. To allow for $M \neq 0$ states, we multiply the basis by

$$\prod_{i=1}^{N}\xi_{m_i}(\boldsymbol{\rho}_i), \tag{5}$$

where

$$\xi_m(\boldsymbol{\rho}) = (x+iy)^m. \tag{6}$$

Thus our nonrestrictive CG function reads as

$$\Phi_M^A(\mathbf{r}) = \mathcal{A}\left\{\left(\prod_{i=1}^{N}\xi_{m_i}(\boldsymbol{\rho}_i)\right)\times \exp\left\{-\frac{1}{2}\sum_{i,j=1}^{N} A_{ij}\boldsymbol{\rho}_i\cdot\boldsymbol{\rho}_j\right\}\right\}, \tag{7}$$

where $M = m_1 + m_2 + \cdots + m_N$, m_i are integers, and $\mathcal{A}$ is an antisymmetrizing operator. This function is coupled with the spin function χ_{SM_S} to form the trial function. The nonlinear parameters are optimized using the stochastic variational method[42,43].

Explicitly Correlated Gaussians (ECG) are very popular in atomic physics and quantum chemistry[43]. The main advantages of ECG bases are: (1) their matrix elements are analytically available for a general N-particle system (2) they are flexible enough to approximate rapidly changing functions (3) the permutation symmetry can be easily imposed and (4) one can make a simple transformation between single-particle and relative coordinate systems. The analytic matrix elements, including those of the Keldysh potential (Eq. 2) which have not been derived before, are presented in the appendix. The basis parameters can be efficiently chosen via the stochastic variational method[42]. In this approach, the variational parameters A_{ij} of the ECG basis (see Eq. 7) are randomly selected, and the parameters giving the lowest variational energy are retained as basis states. This procedure can be fine-tuned into an efficient optimization scheme as described in detail in Refs. 42 and 43.

Ref. 43 provides a thorough review of the applications of the ECG basis in various problems. Benchmark tests presented for atoms with N=2–5 electrons show that the ECG basis can produce up to 10 digit accuracy for 2–3 electron atoms, and while for 2–3 electron atoms the Hylleraas basis is more accurate, for N=4–5 particles, only the ECG basis seems to be feasible. The ECG basis has also proven to be very accurate in calculating weakly bound states. A series of positronic atoms have been predicted using the stochastic variational method with an ECG basis[44,45]. The binding energy in these systems[43] ranges from 0.001 to 0.04 a.u. with weakly bound diffuse structures similar to those studied here. Their complicated clustering structures can be accurately described with the ECG basis.

B. Physical quantities

The following physical quantities will be used to describe the properties of the system and characterize the quality of the wave function. The pair correlation function is defined as

$$C_{pq}(\mathbf{r}) = \frac{2}{N(N-1)} \left\langle \Psi \left| \sum_{i<j}^{N} \delta(\mathbf{r}_i - \mathbf{r}_j - \mathbf{r}) \right| \Psi \right\rangle . \quad (8)$$

Where p and q stand for electrons or holes. Using $C_{pq}(r)$, the radial part of the correlation function, the powers of inter-particle distances are given by

$$\left\langle r_{pq}^{k} \right\rangle = 2\pi \int_0^\infty r^k C_{pq}(r) r \, \mathrm{d}r \, . \quad (9)$$

Distances between particles in a bound system are small, and the particles are confined into distance of a few atomic units. Loosely bound systems tend to be larger, up to several tens of atomic units, but remain finite. In unbound systems, the distances diverge. In order to represent the structure of these systems, correlation functions are reported which are normalized to the number of p-q pairs

$$N_{\text{pairs}}^{pq} = \int_0^\infty C_{pq}^{N}(r) dr. \quad (10)$$

III. RESULTS AND DISCUSSION

In this section, we summarize our results for binding energies within four selected TMDs (Table II) as well as various values corresponding to a range of electron-hole mass ratios $\sigma = m_e/m_h$ and screening lengths r_0. All quantities, unless otherwise specified, are displayed in atomic units. Effective mass and polarizability parameters for the four represented TMDs were obtained from Ref. 30 with an effective mass ratio of $\sigma = 1$ used throughout. Our TMD binding energies agree well with those calculated via the path integral Monte Carlo[35] and diffusion Monte Carlo methods[34]; however, we note that for these methods, statistical errors lead to binding energy uncertainties ranging between 0.2–0.6 meV and 0.1–0.3 meV, respectively. Using parameters listed in Ref. 35, we were generally able to obtain agreement up to three digits (for example, our 484.4 meV for the WSe_2 trion compared to their 484.8(2) meV). For simplicity in calculations with varying σ and r_0, the reduced mass $\mu = (m_e^{-1} + m_h^{-1})^{-1}$ was set to unity, obtaining $m_e = 1 + \sigma$ and $m_h = 1 + 1/\sigma$. Computational details including number of basis functions used and energy convergence may be found in Table I.

Binding energies for excited state biexcitons were calculated with respect to their associated dual exciton decay channels. For a $\sigma = 1$ system (analogous to the positronium molecule), there are four possible bound states: $^1S^e$, $^1S^{e*}$, $^3S^e$, and $^1P^o$. However, while the $^3S^e$ and $^1P^o$ states remain bound in the hydrogenic limit $\sigma \to 0$, the ground state $^1S^e$ and excited state $^1S^{e*}$ merge into states governed by the same symmetry due to the violation of charge parity for $\sigma \neq 1$[46]. Thus, for the biexciton, only three states remain, the $^1S^e$ ground state (X_2) which decays as two ground state excitons, $^3S^e$ (X_2^* ($L = 0$)) which decays as one ground state exciton and one $L = 0$ excited state exciton, and $^1P^o$ (X_2^* ($L = 1$)) which decays as one ground state exciton and one $L = 1$ excited state exciton. Excited states of the trion were determined to be unbound.

The trends for energy dependence on mass ratio are presented in Fig. 1 for the X^-, X_2, X_2^* (L = 0), and X_2^* (L = 1) systems. Note that the exciton is absent from this figure, since its ground state energy does not depend independently on either of the electron or hole effective masses, but only on μ which has been fixed. Our values for the trion and biexciton ground state energies agree well with those of Ref. 32. The dependence of the excited $L = 0$ state biexciton on σ is notably the strongest of the

TABLE I. Number of Gaussian basis functions N_G used and final energy convergence ΔE for each of the represented systems.

System	N_G	ΔE (a.u.)
X	40	10^{-11}
X^-	400	10^{-10}
X_2	500	10^{-8}
$X_2^*(L=0)$	500	10^{-7}
$X_2^*(L=1)$	500	10^{-5}
X_2^-	800	10^{-7}
$X_2^{-*}(L=0)$	800	10^{-6}
$X_2^{-*}(L=1)$	800	10^{-6}

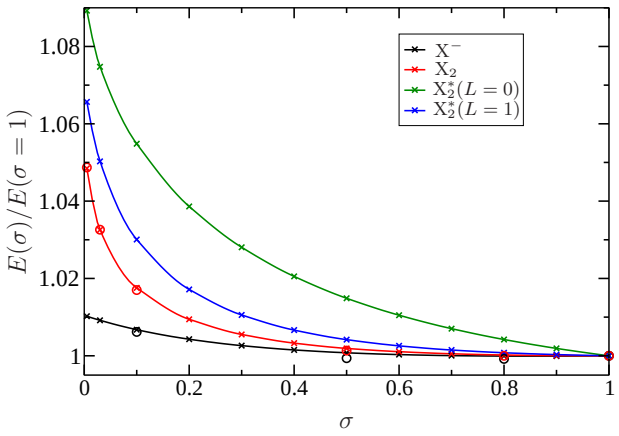

FIG. 1. (Color online) Energy dependence on effective mass ratio $\sigma = m_e/m_h$ for the X^-, X_2, X_2^* (L = 0), and X_2^* (L = 1) systems ranging from the hydrogenic to positronic limits. Results of the present work (solid lines) are compared to results from Ref. 32 (circles) using PIMC approach. Data has been normalized to the values obtained at $\sigma = 1$. Screening length was fixed at $r_0 = 5$ a.u.

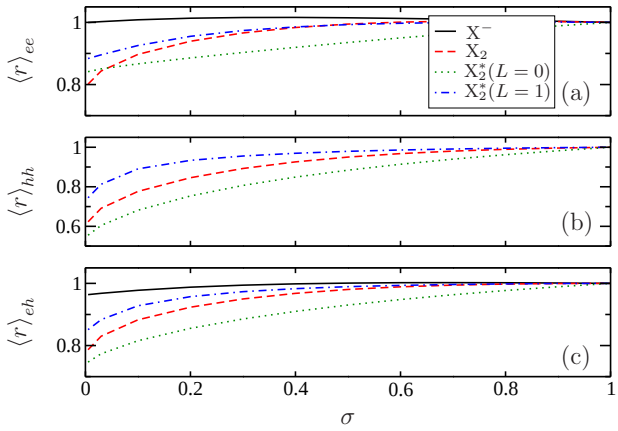

FIG. 2. (Color online) Electron-electron (a), hole-hole (b), and electron-hole (c) inter-particle separations as a function of σ. Data has been normalized to the values obtained at $\sigma = 1$. Screening length was fixed at $r_0 = 5$ a.u.

three biexciton bound states. Inter-particle separation dependence on σ is similarly displayed in Fig. 2. The $L = 0$ biexciton again shows the highest sensitivity to changes in effective mass ratio.

The dependence of energy and binding energy on screening length are presented in Fig. 3. Our results exhibit good agreement with those of Ref. 29 and 32. We note that the biexciton ground state binding energy is larger than that of the trion for small r_0, with a reversal in this relationship coming at screening lengths of $\sim$0.5 a.u. The specific value for this transition point is dependent on the effective mass ratio. In general, for TMD systems, r_0 ranges between 70–100 a.u.; thus, for realistic cases, the biexciton binding energy is expected to be consistently smaller than that of the trion, in contrast with experimental findings. However, the binding energies of the two bound excited state biexcitons are consistently larger than those of the trion. Furthermore, Table II shows excellent agreement between experimental biexciton binding energies and calculated binding energies of the $L = 0$ excited state biexciton. The effect of screening length on inter-particle separation is shown in figure 4. Similar to the findings for varying effective mass ratio, the excited biexcitons react most sensitively to changes in screening length.

The pair correlation functions of these systems, shown in Fig. 5 for the case of monolayer WSe_2, indicate the geometric structure of the formations. The corresponding inter-particle separations are listed in Table III. The ground state biexciton C_{ee} and C_{hh} functions are nearly identical with larger $\langle r\rangle$ values than that of its C_{eh} function, indicative of two excitons orbiting one another. However, the $L = 0$ excited state biexciton exhibits correlation functions which offer a different structural interpretation. The relatively larger $\langle r_{hh}\rangle$ and long tail of the C_{eh} function imply a geometry more similar to that of a negative trion orbited by a hole. The structure of the $L = 1$ excited state of the biexciton, meanwhile, behaves comparably to that of the ground state but with less definitive exciton pairing.

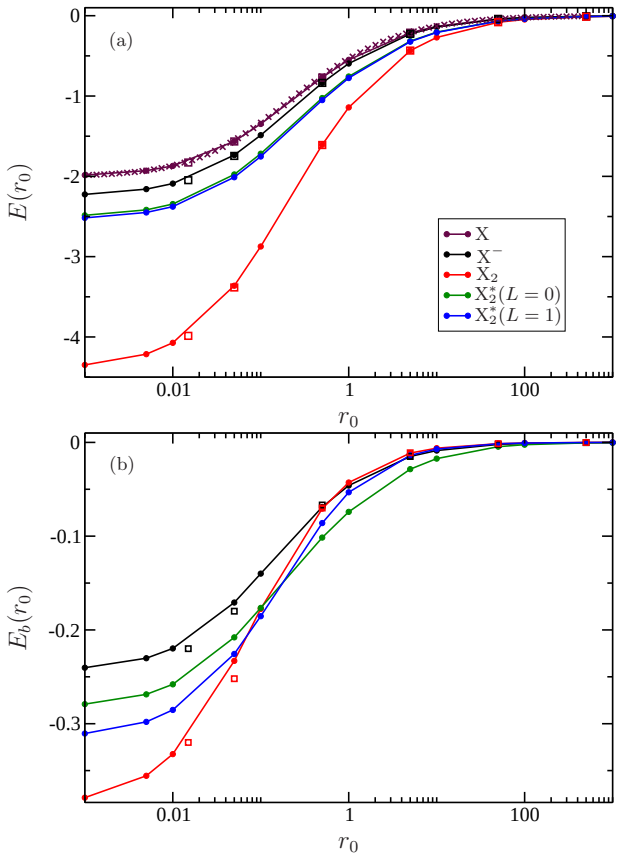

FIG. 3. (Color online) Energy (a) and binding energy (b) dependence on screening length r_0 for the X, X$^-$, and X$_2$ systems. The variational data of Ref. 29, denoted by x's, has been scaled by a factor of 2 in order to account for our $\mu = 1$ convention, as opposed to their $\mu = 1/2$. Also displayed are the PIMC results of Ref. 32 as squares. The effective mass ratios for this data were fixed at 1.

Five-body exciton-trions (X$_2^-$) were also investigated. As displayed in Table II, our binding energy values agree well with those of the PIMC approach[35] in all but this five-body case. This may be a product of the method's constraint on the symmetry of the wave function throughout calculations. Such may, furthermore, explain the significant $MoSe_2$ exciton-trion binding energy discrepancy of Ref. 35, 12.7(4) meV using $\kappa = 2$, with respect to experimental observation upon a SiO_2 substrate, 4 ± 1.5 meV[50]. While in the above mentioned calculations we have neglected any environmental dielectric constant arising from a neighboring substrate, we may simulate the presence of such an environment by setting $\epsilon_{\rm env} = 3.9$, for the case of SiO_2[52], and thus $\kappa = 2.45$ in order to better compare with these experimental observations. Using the same effective mass and 2D polarizability parameters as Ref. 35, we achieved exciton-trion binding energies of 2.4 meV for $\kappa = 2$ and 1.7 meV for $\kappa = 2.45$, both in closer agreement than the PIMC results. To the best of

TABLE II. Comparison of experimental and theoretical TMD excitonic binding energies (meV). Results of the present work are listed in bold. Improved accuracy for values found in Ref. 33 where cited. The $L = 0$ excited state of the exciton-trion was found to be unbound for each choice of TMD.

	System	MoS_2	$MoSe_2$	WS_2	WSe_2
Exper.	X	500[47], 570[48]	550[49]	320[16], 700[18]	370[19]
Theory	X	**555.0**[33], 551.4[34], 526.5[35]	**480.4**[33], 477.8[34], 476.9[35]	**523.5**[33], 519.1[34], 509.8[35]	**470.2**[33], 466.7[34], 456.4[35]
Theory	$X^*(L=0)$	**257.8**[33]	**233.8**[33]	**221.4**[33]	**208.2**[33]
Theory	$X^*(L=1)$	**315.5**[33]	**282.9**[33]	**276.9**[33]	**257.1**[33]
Exper.	X^-	18±1.5[20]	30[5,50]	30[24], 45[21]	30[8,22]
Theory	X^-	**33.7**[33], 33.8[34], 32.0[35]	**28.2**[33], 28.4[34], 27.7[35]	**33.8**[33], 34.0[34], 33.1[35]	**29.5**[33], 29.5[34], 28.5[35]
Exper.	X_2	70[47]	—	65[24]	52[23]
Theory	X_2	**22.5**[33], 22.7[34], 22.7[35]	**18.4**[33], 17.7[34], 19.3[35]	**23.6**[33], 23.3[34], 23.9[35]	**20.2**[33], 20.0[34], 20.7[35]
Theory	$X_2^*(L=0)$	**69.5**[33]	**58.4**[33]	**68.8**[33]	**59.9**[33]
Theory	$X_2^*(L=1)$	**25.3**[51]	**20.2**[51]	**27.3**[51]	**23.2**[51]
Theory	X_2^-	**4.7**, 17.0[35]	**4.3**, 16.4[35]	**3.9**, 14.9[35]	**3.9**, 14.9[35]
Theory	$X_2^{-*}(L=0)$	—	—	—	—
Theory	$X_2^{-*}(L=1)$	**16.0**	**13.6**	**15.5**	**13.4**

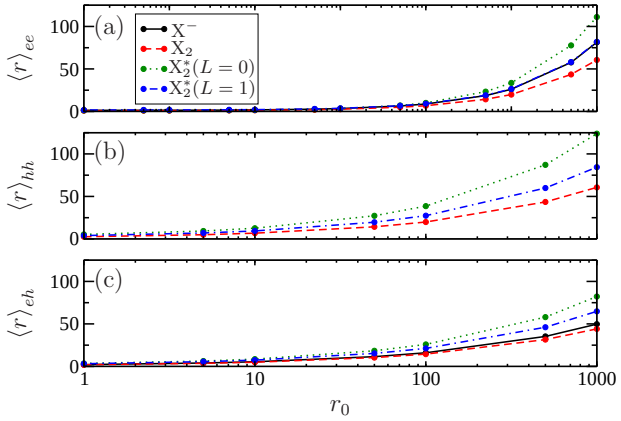

FIG. 4. (Color online) Electron-electron (a), hole-hole (b), and electron-hole (c) inter-particle separation dependence on screening length r_0 for the X, X^-, and X_2 systems. The effective mass ratios for this data were fixed at 1.

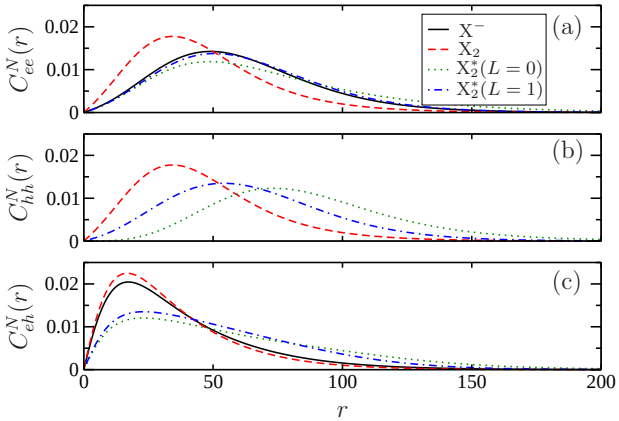

FIG. 5. (Color online) Electron-electron (a), hole-hole (b), and electron-hole (c) correlation functions for excitonic formations within WSe_2.

our knowledge, Ref. 50 is the only experimental finding of such a formation within monolayer TMDs.

Also included in Table II are binding energies for the $L = 1$ excited exciton-trions, which are also determined to be bound. Each of these exciton-trion states were found to exhibit $X + X^-$ decay channels. Correlation functions for ground state and $L = 1$ excited state exciton-trions in WSe_2 are presented in Fig. 6. The namesake is made clear by the large value of $\langle r_{hh}\rangle$ and the extended tail of the C_{eh} function. This implies a trion and exciton orbiting about one another. Alternatively, the excited exciton-trion displays a spatially more condensed structure with a less clear substructure. While the above mentioned exciton-trion cases are determined to be clearly bound, other computations using smaller screening lengths indicate minute binding energies. Thus, such systems often require intensive computational times in order to fully resolve whether the formation is bound. For this reason we report only evidence of these structures in TMDs and leave a more thorough study of their dependence on effective mass ratio and screening length as a subject of future investigation.

Due to the confirmation of bound exciton-trions, the six-body ($eeehhh$) case was subsequently investigated. The energies of these formations in various parameter conditions failed to indicate any allowed bound configurations. This is exemplified by the $r_0 = 100$, $\sigma = 1$ case, whose energy converged to the $X + X_2$ threshold. The correlation functions of this system (see Fig. 7) provide further evidence for this conclusion by exhibiting two peaks, indicative of two separate structures. Similar results were obtained for the above listed choices of TMDs. We conclude, therefore, that five-body formations are the largest excitonic complexes to be expected in 2D materials.

Tables IV–X contain our complete findings for the energies E, binding energies E_b, and interparticle separations $\langle r\rangle$ of the bound exciton, trion, and biexciton sys-

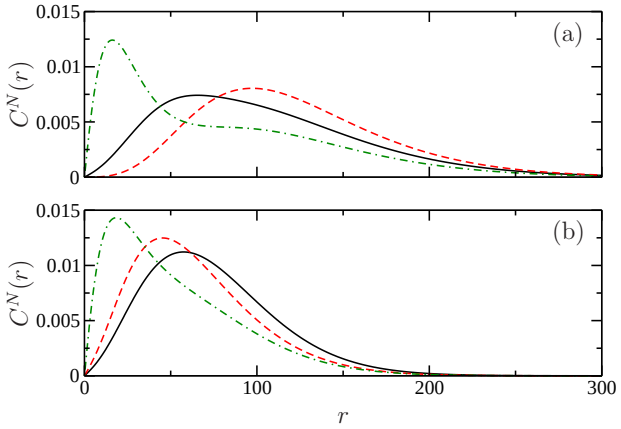

FIG. 6. (Color online) Electron-electron (black, solid), hole-hole (red, dashed), and electron-hole (green, dash-dotted) correlation functions for the ground state (a) and $L = 1$ excited state (b) exciton-trion in monolayer WSe_2.

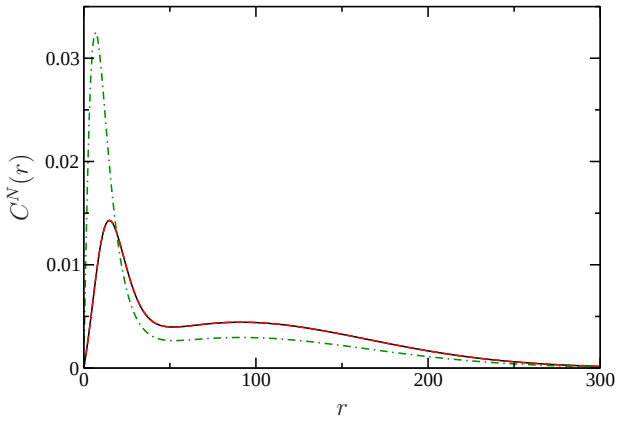

FIG. 7. (Color online) Electron-electron (black, solid), hole-hole (red, dashed), and electron-hole (green, dash-dotted) correlation functions in the six-body system for the case of $r_0 = 100$ and $\sigma = 1$.

tems for a range of screening lengths and effective mass ratios. These values can serve as a benchmark for theory and may guide experiments.

TABLE IV. Exciton ground state and excited state energies in Hartrees.

Exciton (eh)	g.s.	$(L = 0)$	$(L = 1)$
$r_0 = 0\,a_0$	-1.99994	-0.22222	-0.22222
$r_0 = 0.1\,a_0$	-1.34793	-0.19393	-0.21959
$r_0 = 1\,a_0$	-0.54954	-0.13324	-0.17300
$r_0 = 10\,a_0$	-0.13233	-0.05485	-0.06859
$r_0 = 85\,a_0$	-0.02643	-0.01489	-0.01738
$r_0 = 100\,a_0$	-0.02321	-0.01330	-0.01546

TABLE III. Inter-particle separations for various excitonic systems occurring in monolayer WSe_2.

System	$\langle r_{ee}\rangle$	$\langle r_{hh}\rangle$	$\langle r_{eh}\rangle$
X^-	61.034	—	37.930
X_2	46.928	46.928	34.223
$X_2^*(L = 0)$	71.373	87.905	59.714
$X_2^*(L = 1)$	62.683	65.256	51.303
X_2^-	105.069	122.845	78.551
$X_2^{-*}(L = 1)$	74.082	64.502	52.986

TABLE V. Trion (eeh) ground state energies and binding energies in Hartrees.

E	$\sigma = 1$	$\sigma = 0.8$	$\sigma = 0.6$	$\sigma = 0.4$	$\sigma = 0.2$
$r_0 = 0\,a_0$	-2.2432	-2.2517	-2.2662	-2.2930	-2.3553
$r_0 = 0.1\,a_0$	-1.4880	-1.4919	-1.4988	-1.5121	-1.5434
$r_0 = 1\,a_0$	-0.5956	-0.5963	-0.5977	-0.6001	-0.6082
$r_0 = 10\,a_0$	-0.1410	-0.1410	-0.1412	-0.1415	-0.1425
$r_0 = 85\,a_0$	-0.0278	-0.0278	-0.0278	-0.0278	-0.0279
$r_0 = 100\,a_0$	-0.0244	-0.0244	-0.0244	-0.0244	-0.0245
E_b	$\sigma = 1$	$\sigma = 0.8$	$\sigma = 0.6$	$\sigma = 0.4$	$\sigma = 0.2$
$r_0 = 0\,a_0$	-0.2433	-0.2518	-0.2663	-0.2931	-0.3554
$r_0 = 0.1\,a_0$	-0.1401	-0.1440	-0.1509	-0.1642	-0.1955
$r_0 = 1\,a_0$	-0.0461	-0.0468	-0.0482	-0.0506	-0.0587
$r_0 = 10\,a_0$	-0.0087	-0.0087	-0.0089	-0.0092	-0.0102
$r_0 = 85\,a_0$	-0.0014	-0.0014	-0.0014	-0.0014	-0.0015
$r_0 = 100\,a_0$	-0.0012	-0.0012	-0.0012	-0.0012	-0.0013

TABLE VI. Biexciton ground state energies and binding energies in Hartrees.

E	$\sigma = 1$	$\sigma = 0.8$	$\sigma = 0.6$	$\sigma = 0.4$	$\sigma = 0.2$
$r_0 = 0\,a_0$	-4.3857	-4.3887	-4.4016	-4.4351	-4.5290
$r_0 = 0.1\,a_0$	-2.8736	-2.8750	-2.8810	-2.8968	-2.9410
$r_0 = 1\,a_0$	-1.1419	-1.1422	-1.1436	-1.1474	-1.1577
$r_0 = 10\,a_0$	-0.2708	-0.2708	-0.2710	-0.2716	-0.2730
$r_0 = 85\,a_0$	-0.0537	-0.0537	-0.0537	-0.0538	-0.0540
$r_0 = 100\,a_0$	-0.0471	-0.0471	-0.0471	-0.0472	-0.0474
E_b	$\sigma = 1$	$\sigma = 0.8$	$\sigma = 0.6$	$\sigma = 0.4$	$\sigma = 0.2$
$r_0 = 0\,a_0$	-0.3858	-0.3888	-0.4016	-0.4352	-0.5290
$r_0 = 0.1\,a_0$	-0.1776	-0.1790	-0.1850	-0.2008	-0.2450
$r_0 = 1\,a_0$	-0.0428	-0.0431	-0.0445	-0.0483	-0.0587
$r_0 = 10\,a_0$	-0.0061	-0.0062	-0.0064	-0.0069	-0.0083
$r_0 = 85\,a_0$	-0.0008	-0.0008	-0.0009	-0.0009	-0.0011
$r_0 = 100\,a_0$	-0.0007	-0.0007	-0.0007	-0.0008	-0.0009

TABLE VII. Biexciton ($L = 0$) excited state energies and binding energies in Hartrees.

E	$\sigma = 1$	$\sigma = 0.8$	$\sigma = 0.6$	$\sigma = 0.4$	$\sigma = 0.2$
$r_0 = 0\,a_0$	-2.5043	-2.5058	-2.5124	-2.5295	-2.5747
$r_0 = 0.1\,a_0$	-1.7184	-1.7227	-1.7314	-1.7486	-1.7874
$r_0 = 1\,a_0$	-0.7568	-0.7605	-0.7661	-0.7754	-0.7929
$r_0 = 10\,a_0$	-0.2045	-0.2052	-0.2063	-0.2081	-0.2114
$r_0 = 85\,a_0$	-0.0442	-0.0443	-0.0444	-0.0447	-0.0451
$r_0 = 100\,a_0$	-0.0390	-0.0391	-0.0392	-0.0394	-0.0398
E_b	$\sigma = 1$	$\sigma = 0.8$	$\sigma = 0.6$	$\sigma = 0.4$	$\sigma = 0.2$
$r_0 = 0\,a_0$	-0.2822	-0.2836	-0.2902	-0.3073	-0.3525
$r_0 = 0.1\,a_0$	-0.1765	-0.1809	-0.1896	-0.2068	-0.2456
$r_0 = 1\,a_0$	-0.0741	-0.0777	-0.0833	-0.0926	-0.1102
$r_0 = 10\,a_0$	-0.0173	-0.0180	-0.0191	-0.0209	-0.0242
$r_0 = 85\,a_0$	-0.0029	-0.0030	-0.0031	-0.0034	-0.0038
$r_0 = 100\,a_0$	-0.0025	-0.0025	-0.0027	-0.0029	-0.0033

TABLE VIII. Biexciton ($L = 1$) excited state energies in Hartrees.

E	$\sigma = 1$	$\sigma = 0.8$	$\sigma = 0.6$	$\sigma = 0.4$	$\sigma = 0.2$
$r_0 = 0\,a_0$	-3.3762	-3.3544	-3.3426	-3.3730	-3.3780
$r_0 = 0.1\,a_0$	-1.5676	-1.7525	-1.7550	-1.7619	-1.7839
$r_0 = 1\,a_0$	-0.7761	-0.7759	-0.7765	-0.7787	-0.7852
$r_0 = 10\,a_0$	-0.2081	-0.2081	-0.2082	-0.2086	-0.2097
$r_0 = 85\,a_0$	-0.0447	-0.0447	-0.0447	-0.0447	-0.0449
$r_0 = 100\,a_0$	-0.0394	-0.0394	-0.0394	-0.0394	-0.0396
E_b	$\sigma = 1$	$\sigma = 0.8$	$\sigma = 0.6$	$\sigma = 0.4$	$\sigma = 0.2$
$r_0 = 0\,a_0$	-0.3138	-0.3161	-0.3228	-0.3383	-0.3850
$r_0 = 0.1\,a_0$	-0.1854	-0.1871	-0.1920	-0.2031	-0.2304
$r_0 = 1\,a_0$	-0.0532	-0.0543	-0.0562	-0.0603	-0.0709
$r_0 = 10\,a_0$	-0.0071	-0.0073	-0.0077	-0.0084	-0.0103
$r_0 = 85\,a_0$	-0.0009	-0.0009	-0.0009	-0.0010	-0.0013
$r_0 = 100\,a_0$	-0.0007	-0.0007	-0.0008	-0.0009	-0.0011

TABLE IX. Trion interparticle separation in Bohr radii.

$\langle r_{ee} \rangle$	$\sigma = 1$	$\sigma = 0.8$	$\sigma = 0.6$	$\sigma = 0.4$	$\sigma = 0.2$
$r_0 = 0\,a_0$	1.304	1.332	1.361	1.388	1.406
$r_0 = 0.1\,a_0$	1.781	1.812	1.842	1.868	1.881
$r_0 = 1\,a_0$	3.387	3.423	3.455	3.478	3.479
$r_0 = 10\,a_0$	8.755	8.808	8.849	8.868	8.839
$r_0 = 85\,a_0$	24.097	24.196	24.264	24.274	24.167
$r_0 = 100\,a_0$	26.084	26.189	26.261	26.269	26.153
$\langle r_{eh} \rangle$	$\sigma = 1$	$\sigma = 0.8$	$\sigma = 0.6$	$\sigma = 0.4$	$\sigma = 0.2$
$r_0 = 0\,a_0$	0.857	0.868	0.879	0.887	0.888
$r_0 = 0.1\,a_0$	1.150	1.161	1.171	1.176	1.172
$r_0 = 1\,a_0$	2.146	2.157	2.163	2.161	2.142
$r_0 = 10\,a_0$	5.455	5.462	5.459	5.435	5.374
$r_0 = 85\,a_0$	14.839	14.839	14.811	14.731	14.558
$r_0 = 100\,a_0$	16.052	16.052	16.020	15.932	15.745

TABLE X. Biexciton interparticle separation in Bohr radii.

$\langle r_{ee} \rangle$	$\sigma = 1$	$\sigma = 0.8$	$\sigma = 0.6$	$\sigma = 0.4$	$\sigma = 0.2$
$r_0 = 0\,a_0$	0.905	0.912	0.913	0.900	0.860
$r_0 = 0.1\,a_0$	1.296	1.304	1.302	1.282	1.223
$r_0 = 1\,a_0$	2.578	2.590	2.583	2.539	2.424
$r_0 = 10\,a_0$	6.739	6.767	6.744	6.627	6.330
$r_0 = 85\,a_0$	18.356	18.427	18.363	18.047	17.246
$r_0 = 100\,a_0$	19.851	19.928	19.859	19.517	18.650
$\langle r_{hh} \rangle$	$\sigma = 1$	$\sigma = 0.8$	$\sigma = 0.6$	$\sigma = 0.4$	$\sigma = 0.2$
$r_0 = 0\,a_0$	0.905	0.891	0.866	0.817	0.722
$r_0 = 0.1\,a_0$	1.296	1.280	1.246	1.183	1.060
$r_0 = 1\,a_0$	2.578	2.550	2.491	2.377	2.160
$r_0 = 10\,a_0$	6.739	6.670	6.526	6.247	5.715
$r_0 = 85\,a_0$	18.356	18.174	17.790	17.049	15.635
$r_0 = 100\,a_0$	19.851	19.654	19.239	18.438	16.912
$\langle r_{eh} \rangle$	$\sigma = 1$	$\sigma = 0.8$	$\sigma = 0.6$	$\sigma = 0.4$	$\sigma = 0.2$
$r_0 = 0\,a_0$	0.703	0.701	0.694	0.677	0.640
$r_0 = 0.1\,a_0$	0.978	0.976	0.967	0.945	0.896
$r_0 = 1\,a_0$	1.903	1.898	1.881	1.840	1.752
$r_0 = 10\,a_0$	4.920	4.909	4.866	4.764	4.547
$r_0 = 85\,a_0$	13.351	13.322	13.206	12.933	12.355
$r_0 = 100\,a_0$	14.435	14.405	14.280	13.984	13.360

IV. CONCLUSIONS

We have applied the stochastic variational method using a accurate correlated Gaussian basis to the calculation of energies and geometries for two- to six-body excitonic formations in transition metal dichalcogenides. Our results lie in good agreement with similar theoretical

effective mass model findings for the majority of these systems, as well as existing experimental binding energies for the cases of the exciton, trion, and exciton-trion. Our disagreement with the PIMC approach in the case of the exciton-trion may be due to its constraint on the symmetry of the wave function.

As highlighted in our previous work, there exists a discrepancy between theoretical and experimentally found biexciton binding energies; however, the $L = 0$ excited state of the biexciton appears to match well with experimental values. This implies that the formations being observed could be these excited states. Also determined to be bound are the $L = 1$ excited state of the biexciton and exciton-trion. By examining the inter-particle correlation functions, the substructure of these excited systems have been investigated. For example, the $L = 0$ excited biexciton has notably been determined to resemble a negative trion with an orbiting hole. Our findings indicate that no systems containing more than five particles are to be expected in TMDs.

Furthermore, the dependence of the binding energy and structure of these systems with respect to screening length and effective mass ratio have been investigated. Our findings for ground state excitons, trions, and biexcitons agree well with previous theoretical work. Unique to this paper, however, is the characterization of excited biexciton states which are expected to be more sensitive to changes in these parameters. The dependence of the bound exciton-trion states on these parameters have been omitted due to computational limitations and is left as the subject of future investigation. Such would become pertinent in the surfacing of further experimental data.

We have shown that while experiments agree well with calculated ground state binding energies of excitonic formations within TMDs, the theory allows for additional excited excitonic structures which have not been observed. We propose that this discrepancy may be explained as a lack of spectral resolution necessary to distinguish the individual signals of these formations; for instance, the trion, ground state biexciton, and $L = 1$ excited state biexciton are predicted to have similar binding energies. In addition, experiments may not have targeted these hitherto unknown multiple bound states. Further experimental and theoretical work is needed to more fully explain this discrepancy.

This work has been supported by the National Science Foundation (NSF) under Grants No. Phy 1314463 and No. IIA126117.

[1] K. S. Novoselov, A. K. Geim, S. V. Morozov, D. Jiang, Y. Zhang, S. V. Dubonos, I. V. Grigorieva, and A. A. Firsov, Science **306**, 666 (2004).

[2] B. Radisavljevic, A. Radenovic, J. Brivio, V. Giacometti, and A. Kis, Nat. Nanotechnol. **6**, 147150 (2011).

[3] Lopez-Sanchez Oriol, Lembke Dominik, Kayci Metin, Radenovic Aleksandra, and Kis Andras, Nat. Nanotechnol. **8**, 497501 (2013).

[4] Mak Kin Fai, He Keliang, Lee Changgu, Lee Gwan Hyoung, Hone James, Heinz Tony F., and Shan Jie, Nat. Mater. **12**, 207211 (2013).

[5] Ross Jason S., Wu Sanfeng, Yu Hongyi, Ghimire Nirmal J., Jones Aaron M., Aivazian Grant, Yan Jiaqiang, Mandrus David G., Xiao Di, Yao Wang, and Xu Xiaodong, Nat. Commun. **4**, 1474 (2013).

[6] Y. Lin, X. Ling, L. Yu, S. Huang, A. L. Hsu, Y.-H. Lee, J. Kong, M. S. Dresselhaus, and T. Palacios, Nano Lett. **14**, 55695576 (2014).

[7] Xu Xiaodong, Yao Wang, Xiao Di, and Heinz Tony F., Nat. Phys. **10**, 343350 (2014).

[8] Jones Aaron M., Yu Hongyi, Ghimire Nirmal J., Wu Sanfeng, Aivazian Grant, Ross Jason S., Zhao Bo, Yan Jiaqiang, Mandrus David G., Xiao Di, Yao Wang, and Xu Xiaodong, Nat. Nanotechnol. **8**, 634638 (2013).

[9] K. S. Novoselov, V. I. Fal'ko, L. Colombo, P. R. Gellert, M. G. Schwab, and K. Kim, Nature **490**, 192 (2012).

[10] D. Jariwala, V. K. Sangwan, L. J. Lauhon, T. J. Marks, and M. C. Hersam, ACS Nano **8**, 1102 (2014).

[11] M. Chhowalla, H. S. Shin, G. Eda, L.-J. Li, K. P. Loh, and H. Zhang, Nat. Chem. **5**, 263 (2013).

[12] J. Wilson and A. Yoffe, Adv. Phys. **18**, 193 (1969).

[13] Q. H. Wang, K. Kalantar-Zadeh, A. Kis, J. N. Coleman, and M. S. Strano, Nat. Nanotechnol. **7**, 699 (2012).

[14] J. Wilson, F. D. Salvo, and S. Mahajan, Adv. Phys. **24**, 117 (1975).

[15] K. F. Mak, C. Lee, J. Hone, J. Shan, and T. F. Heinz, Phys. Rev. Lett. **105**, 136805 (2010).

[16] A. Chernikov, T. C. Berkelbach, H. M. Hill, A. Rigosi, Y. Li, O. B. Aslan, D. R. Reichman, M. S. Hybertsen, and T. F. Heinz, Phys. Rev. Lett. **113**, 076802 (2014).

[17] M. M. Ugeda, A. J. Bradley, S.-F. Shi, F. H. da Jornada, Y. Zhang, D. Y. Qiu, W. Ruan, S.-K. Mo, Z. Hussain, Z.-X. Shen, F. Wang, S. G. Louie, and M. F. Crommie, Nat. Mater. **13**, 1091 (2014).

[18] Ye Ziliang, Cao Ting, O'Brien Kevin, Zhu Hanyu, Yin Xiaobo, Wang Yuan, Louie Steven G., and Zhang Xiang, Nature **513**, 214218 (2014).

[19] K. He, N. Kumar, L. Zhao, Z. Wang, K. F. Mak, H. Zhao, and J. Shan, Phys. Rev. Lett. **113**, 026803 (2014).

[20] K. F. Mak, K. He, C. Lee, G. H. Lee, J. Hone, T. F. Heinz, and J. Shan, Nat. Mater. **12**, 207 (2013).

[21] B. Zhu, H. Zeng, J. Dai, Z. Gong, and X. Cui, Proc. Natl. Acad. Sci. U.S.A. **111**, 11606 (2014).

[22] G. Wang, L. Bouet, D. Lagarde, M. Vidal, A. Balocchi, T. Amand, X. Marie, and B. Urbaszek, Phys. Rev. B **90**, 075413 (2014).

[23] Y. You, X.-X. Zhang, T. C. Berkelbach, M. S. Hybertsen, D. R. Reichman, and T. F. Heinz, Nat. Phys. **11**, 477 (2015).

[24] G. Plechinger, P. Nagler, J. Kraus, N. Paradiso, C. Strunk, C. Schller, and T. Korn, Phys. Status Solidi RRL **9**, 457 (2015).

[25] M. A. Lampert, Phys. Rev. Lett. **1**, 450 (1958).

[26] J. Usukura, Y. Suzuki, and K. Varga, Phys. Rev. B **59**, 5652 (1999).

[27] C. Riva, F. M. Peeters, and K. Varga, Phys. Rev. B **61**,

13873 (2000).
[28] L. V. Keldysh, JETP Lett. **29**, 658 (1979).
[29] E. Prada, J. V. Alvarez, K. L. Narasimha-Acharya, F. J. Bailen, and J. J. Palacios, Phys. Rev. B **91**, 245421 (2015).
[30] T. C. Berkelbach, M. S. Hybertsen, and D. R. Reichman, Phys. Rev. B **88**, 045318 (2013).
[31] B. Ganchev, N. Drummond, I. Aleiner, and V. Fal'ko, Phys. Rev. Lett. **114**, 107401 (2015).
[32] K. A. Velizhanin and A. Saxena, Phys. Rev. B **92**, 195305 (2015).
[33] D. K. Zhang, D. W. Kidd, and K. Varga, Nano Lett. **15**, 7002 (2015).
[34] M. Z. Mayers, T. C. Berkelbach, M. S. Hybertsen, and D. R. Reichman, Phys. Rev. B **92**, 161404 (2015).
[35] I. Kylänpää and H.-P. Komsa, Phys. Rev. B **92**, 205418 (2015).
[36] K. Varga and J. A. Driscoll, *Computational Nanoscience* (Cambridge University Press, 2011).
[37] S. Bubin, F. Leonarski, M. Stanke, and L. Adamowicz, Chem. Phys. Lett. **477**, 12 (2009).
[38] D. B. Kinghorn and R. D. Poshusta, Phys. Rev. A **47**, 3671 (1993).
[39] P. M. Kozlowski and L. Adamowicz, Phys. Rev. A **48**, 1903 (1993).
[40] T. Takagahara, Phys. Rev. B **47**, 4569 (1993).
[41] P. Cudazzo, I. V. Tokatly, and A. Rubio, Phys. Rev. B **84**, 085406 (2011).
[42] Y. Suzuki and K. Varga, *Stochastic Variational Approach to Quantum-Mechanical Few-Body Problems* (Springer, 1998).
[43] J. Mitroy, S. Bubin, W. Horiuchi, Y. Suzuki, L. Adamowicz, W. Cencek, K. Szalewicz, J. Komasa, D. Blume, and K. Varga, Rev. Mod. Phys. **85**, 693 (2013).
[44] R. Krivec, V. B. Mandelzweig, and K. Varga, Phys. Rev. A **61**, 062503 (2000).
[45] K. Varga, Phys. Rev. Lett. **83**, 5471 (1999).
[46] Y. Suzuki and J. Usukura, Nucl. Instr. Meth. Phys. Res. B **171**, 6780 (2000).
[47] C. Mai, A. Barrette, Y. Yu, Y. G. Semenov, K. W. Kim, L. Cao, and K. Gundogdu, Nano Lett. **14**, 202206 (2014).
[48] Klots A. R., Newaz A. K. M., Wang Bin, Prasai D., Krzyzanowska H., Lin Junhao, Caudel D., Ghimire N. J., Yan J., Ivanov B. L., Velizhanin K. A., Burger A., Mandrus D. G., Tolk N. H., Pantelides S. T., and Bolotin K. I., Sci. Rep. **4** (2014).
[49] Ugeda Miguel M., Bradley Aaron J., Shi Su-Fei, da Jornada Felipe H., Zhang Yi, Qiu Diana Y., Ruan Wei, Mo Sung-Kwan, Hussain Zahid, Shen Zhi-Xun, Wang Feng, Louie Steven G., and Crommie Michael F., Nat. Mater. **13**, 10911095 (2014).
[50] A. Singh, G. Moody, S. Wu, Y. Wu, N. J. Ghimire, J. Yan, D. G. Mandrus, X. Xu, and X. Li, Phys. Rev. Lett. **112**, 216804 (2014).
[51] Incorrectly reported binding energies for the $L = 1$ excited biexciton are rectified in this publication.
[52] P. Gray, *Analysis and Design of Analog Integrated Circuits* (Wiley, New York, 2009).
[53] K. Varga, Comput. Phys. Commun. **179**, 591 (2008).

Appendix

In this appendix, we derive analytic expressions for the necessary ECG-basis potential matrix elements. In order to calculate these matrices we take advantage of the generating functions (as explained in further detail within Ref. 53)

$$G^A_{\mathbf{t}}(\mathbf{r}) = \exp\left\{-\frac{1}{2}\mathbf{r}A\mathbf{r} + \mathbf{t}\mathbf{r}\right\}, \tag{A.1}$$

where $\mathbf{t} = (\mathbf{t}_1, \ldots, \mathbf{t}_N)$ and $\mathbf{t}_k = t_k(1, i\alpha_k)$ and $\alpha_k = \pm 1$ and t_k is a variable to be used in taking the derivative of the generating function. The basis functions can be expressed in terms of these generating functions as

$$\begin{aligned}\Phi^A_m(\mathbf{r}) &= \prod_{k=1}^{N}(x_k + iy_k)^{m_k}\exp\left\{-\frac{1}{2}\mathbf{r}A\mathbf{r}\right\} \\ &= \prod_{k=1}^{N}\frac{\partial^{m_k}}{\partial t_k^{m_k}}G^A_{\mathbf{t}}(\mathbf{r})\bigg|_{\mathbf{t}=0}.\end{aligned} \tag{A.2}$$

Now, we need only calculate the matrix elements with respect to the generating functions, since the matrix elements of an arbitrary operator $\hat{\mathcal{B}}$ are given by

$$\langle\Phi^A_m|\hat{\mathcal{B}}|\Phi^{A'}_{m'}\rangle = \prod_{k=1}^{N}\frac{\partial^{m_k}}{\partial t_k^{m_k}}\prod_{k'=1}^{N}\frac{\partial^{m'_k}}{\partial t_k'^{\,m'_k}}\langle G^A_{\mathbf{t}}|\hat{\mathcal{B}}|G^{A'}_{\mathbf{t}'}\rangle\bigg|_{\mathbf{t}=0,\mathbf{t}'=0} \tag{A.3}$$

The calculation of the matrix elements of the kinetic energy and the overlap of the basis functions are presented in Ref. 26, 42, 43, and 53. For spherically symmetric potentials, this calculation reduces to the computation of the 1D integral

$$I \equiv \int_0^\infty r^{2n+1}e^{-cr^2}V(r)\,\mathrm{d}r\,, \tag{A.4}$$

where r_0 and c are positive real constants, and n is a nonnegative integer. We can exploit the fact that the screened Coulomb potential,

$$V(r) = \frac{\pi}{2r_0}\left[H_0\left(\frac{r}{r_0}\right) - Y_0\left(\frac{r}{r_0}\right)\right], \tag{A.5}$$

has a particularly simple momentum-space representation (i.e., 2D Fourier transform)[23] :

$$\begin{aligned}\mathcal{F}_{2\mathrm{D}}[V](\mathbf{k}) &= \int V(\mathbf{r})e^{-i\mathbf{k}\cdot\mathbf{r}}\mathrm{d}^2\mathbf{r} \\ &= \int_0^{2\pi}\int_0^\infty V(r)e^{-ikr\cos\theta}r\,\mathrm{d}r\,\mathrm{d}\theta \\ &= 2\pi\int_0^\infty rJ_0(kr)V(r)\,\mathrm{d}r \\ &= \frac{2\pi}{k(1+r_0k)}.\end{aligned} \tag{A.6}$$

Here, the second equality follows by expressing $\mathbf{r}$ in polar coordinates (r, θ) with polar axis aligned with $\mathbf{k}$, and the third equality follows from the identity

$$\int_0^{2\pi} e^{\pm ikr\cos\theta}\,\mathrm{d}\theta = 2\pi J_0(kr), \tag{A.7}$$

where J_0 is a Bessel function of the first kind. To make use of this representation, we convert I into a 2D integral by introducing angular dependence

$$I = \frac{1}{2\pi}\int_0^{2\pi}\int_0^\infty r^{2n}e^{-cr^2}V(r)\;r\,\mathrm{d}r\,\mathrm{d}\theta \tag{A.8}$$

and apply the Fourier transform property

$$\int f(\mathbf{r})g(\mathbf{r})\,\mathrm{d}^2\mathbf{r} = \int \mathcal{F}_{2\mathrm{D}}[f](\mathbf{k})\;\mathcal{F}^{-1}_{2\mathrm{D}}[g](\mathbf{k})\,\mathrm{d}^2\mathbf{k} \tag{A.9}$$

with $f = V$ and $g(\mathbf{r}) = r^{2n}e^{-cr^2}$. This requires the computation of $\mathcal{F}^{-1}_{2\mathrm{D}}[g]$, as follows:

$$\begin{aligned}\mathcal{F}^{-1}_{2\mathrm{D}}[g](\mathbf{k}) &= \frac{1}{4\pi^2}\int g(\mathbf{r})e^{i\mathbf{k}\cdot\mathbf{r}}\mathrm{d}^2\mathbf{r} \\ &= \frac{1}{4\pi^2}\int_0^{2\pi}\int_0^\infty g(r)e^{ikr\cos\theta}r\,\mathrm{d}r\,\mathrm{d}\theta \\ &= \frac{1}{2\pi}\int_0^\infty rJ_0(kr)g(r)\,\mathrm{d}r \\ &= \frac{n!}{4^n\pi\alpha^{n-1}}e^{-\alpha k^2}L_n(\alpha k^2).\end{aligned} \tag{A.10}$$

Here, $\alpha = 1/(4c)$, and L_n is the nth Laguerre polynomial, given by

$$L_n(x) = \sum_{j=0}^{n}\frac{(-1)^j}{j!}\binom{n}{j}x^j. \tag{A.11}$$

Thus, our desired integral is

$$\begin{aligned}I &= \frac{1}{2\pi}\int\mathcal{F}_{2\mathrm{D}}[V](\mathbf{k})\;\mathcal{F}^{-1}_{2\mathrm{D}}[g](\mathbf{k})\,\mathrm{d}^2\mathbf{k} \\ &= \frac{n!}{4^n\pi\alpha^{n-1}}\int_0^{2\pi}\int_0^\infty\frac{e^{-\alpha k^2}L_n(\alpha k^2)}{k(1+r_0k)}\;k\,\mathrm{d}k\,\mathrm{d}\theta \\ &= \frac{2n!}{4^n\alpha^{n-1}}\int_0^\infty\frac{e^{-\alpha k^2}L_n(\alpha k^2)}{1+r_0k}\,\mathrm{d}k \\ &= \frac{2n!}{4^n\alpha^{n-1}}\sum_{j=0}^{n}\frac{(-\alpha)^j}{j!}\binom{n}{j}\int_0^\infty\frac{k^{2j}e^{-\alpha k^2}}{1+r_0k}\,\mathrm{d}k\,.\end{aligned} \tag{A.12}$$

At this point, there are two natural routes by which to proceed. One approach is to consider the sequence of integrals

$$I_m = \int_0^\infty\frac{k^{2m}e^{-\alpha k^2}}{1+r_0k}\,\mathrm{d}k\,. \tag{A.13}$$

It is possible to directly obtain a closed form for I_m in terms of the incomplete Γ function, but this is expensive

to numerically evaluate. Instead, observe that

$$\begin{aligned} r_0^2 I_{m+1} - I_m &= \int_0^\infty \frac{r_0^2 k^2 - 1}{1 + r_0 k} k^{2m} e^{-\alpha k^2} \, \mathrm{d}k \\ &= \int_0^\infty (1 - r_0 k) k^{2m} e^{-\alpha k^2} \, \mathrm{d}k \\ &= \frac{1}{2\alpha^{m+1}} \left[r_0 m! - \sqrt{\alpha} \Gamma\left(m + \frac{1}{2}\right) \right] \end{aligned} \tag{A.14}$$

is a linear first-order recurrence relation for I_m, with initial condition

$$I_0 = \frac{1}{2r_0} \left[2\sqrt{\pi} F(\gamma) - e^{-\gamma^2} \mathrm{Ei}(\gamma^2) \right]. \tag{A.15}$$

Here, $\gamma = \sqrt{\alpha}/r_0$, F is the Dawson function, and Ei is the exponential integral. This linear recurrence provides an efficient numerical technique for the evaluation of the integral sequence I_m, and by Eq. A.12, the desired integral I.

As an important implementation detail, note that $\mathrm{Ei}(x)$ grows (sub)exponentially while e^{-x} decays exponentially as $x \to \infty$; thus, the product $e^{-\gamma^2}\mathrm{Ei}(\gamma^2)$ appearing in Eq. A.15 may contain substantial numerical error due to destructive cancellation when γ is large. Numerical methods exist for the direct evaluation of the scaled exponential integral $e^{-x}\mathrm{Ei}(x)$, and are provided by some libraries; these should be preferred when available.

Alternatively, we may also consider power-series expansion of $(1 + r_0 k)^{-1}$, which occurs in the denominator of I_m:

$$\begin{aligned} I_m &= \int_0^\infty k^{2m} e^{-\alpha k^2} \sum_{b=0}^\infty (-r_0 k)^b \, \mathrm{d}k \\ &= \sum_{b=0}^\infty (-r_0)^b \int_0^\infty k^{2m+b} e^{-\alpha k^2} \, \mathrm{d}k \\ &= \sum_{b=0}^\infty (-r_0)^b \left(\frac{\Gamma\left(\frac{b+1}{2} + m\right)}{2\alpha^{\frac{1}{2}(2m+b+1)}} \right) \\ &= \frac{1}{2\alpha^{m+\frac{1}{2}}} \sum_{b=0}^\infty \left(-\frac{r_0}{\sqrt{\alpha}} \right)^b \Gamma\left(\frac{b+1}{2} + m \right). \end{aligned}$$

While the resulting series has zero radius of convergence (since the Γ function asymptotically dominates the general term), for small $r_0\sqrt{c}$ the first several partial sums provide excellent approximation to the exact result.